J Petrol Explor Prod Technol (2016) 6:533–543
DOI 10.1007/s13202-015-0200-z

ORIGINAL PAPER - EXPLORATION ENGINEERING

Numerical simulation of resistivity LWD tool based on higher-order vector finite element

Li Hui[1] · **Shen Yi-ze**[2] · **Zhu Xi-fang**[1]

Received: 28 October 2014 / Accepted: 9 August 2015 / Published online: 27 August 2015

Abstract Numerical simulation of resistivity logging-while-drilling (LWD) tool response in complex borehole environments is of great importance for interpretation of measurement data and characterization of oil reservoirs. The simulation results can provide important theoretical guidance for designing novel electrical logging instruments and interpreting real-time logging data. In this paper, higher-order vector finite element method had been used to investigate the resistivity LWD tool response by changing coils spacing, transmitting frequency and structure of antenna system in the anisotropic formation. Numerical simulation results indicate that the change of T–R_1 spacing is an obvious influence on the investigation depth and detecting precision of the resistivity LWD tool, and the change of R_1–R_2 spacing can affect the resolution of the thin-layer distinguish. The change of transmitting frequency can improve the resolution of low-resistivity formation and high-resistivity formation of resistivity LWD tool. The change of the structure of the antenna system can provide accurate geosteering drilling information to directional resistivity LWD tool. Simulation results also indicated that the higher-order vector finite element method has good convergence speed and calculation accuracy and it is suitable to simulate the response of resistivity LWD tools.

✉ Li Hui
toobage@163.com

[1] School of Electric Engineering and Photoelectric Engineering, Changzhou Institute of Technology, Changzhou 213002, China

[2] CNPC Bohai Drilling Engineering Ltd. Co., DDDC, Tianjin 300280, China

Keywords Numerical simulation · Resistivity LWD · Higher-order vector finite element · Antenna system · Geosteering drilling

Introduction

Resistivity LWD tool has become an important facility for real-time well-site data acquisition and interpretation, scene decision making, and geological-oriented drilling guidance. Therefore, it plays an increasingly important role in geosteer drilling, real-time formation comparative evaluation and complex oil reservoir development (Shi 2002). As a result, it is important to increase the measuring accuracy and improve the response features of the resistivity LWD tool. Novel numerical simulation technology of resistivity LWD tool response can provide important theoretical guidance for designing high-accuracy electrical logging instruments and building accurate measurement data interpretation method. So it is of important significance to research high effective numerical simulation algorithms of resistivity LWD tool (Sun et al. 2008; Wei et al. 2010).

Many researches have been conducted to develop numerical simulation algorithms for resistivity LWD tool response in recent years (Gao et al. 2010). The most frequently used algorithms in the forward numerical simulation include finite difference method (Teixeiraa and Chew 2004), integral equation method (Hue et al. 2005), numerical mode matching method (Tan et al. 2007), successive approximation method (Gao et al. 2010), transmission line matrix (Li and Liu 2005), FFT transform method (Zhang and Liu 2003), and finite element method (FEM) (Wang et al. 2006). Although these conventional algorithms have their own strong points in the field of

forward numerical simulation of the resistivity LWD tool response, approximation accuracy and convergence speed are still not enough for these algorithms. In addition, the weakness of low computational efficiency, poor iterative performance and dynamic numerical simulation difficulties also restrict these conventional algorithms to be used further in wider fields. The higher-order vector FEM was introduced in 1980s by Babuška and Suri (Demkowicz et al. 2002; Pardo et al.2007), and used in simulation of resistivity logging instrument response by Demkowicz and Vardapetyan (Šolín et al. 2008; Tomáš et al. 2007). Its advantage over other numerical methods is an unconditional exponential convergence, even for problems with singular solutions. Now, higher-order vector FEM theoretical foundations are well established and the algorithm is well used for oil field (Chen et al. 2011; Ma et al. 2012; Li et al. 2012). As the formations surrounding the borehole having influencing factors, the change of well geological conditions and complex stratigraphic geometrical structures become more complex, it makes the numerical modeling of the apparatus responses a demanding business in terms of computation speed and accuracy. Higher-order vector FEM in the convergence speed and the calculation accuracy have certain advantages. Therefore, higher-order vector FEM is suitable for simulating the responses of the resistivity LWD tool. Thus, based on the higher-order vector FEM, the influence of T–R_1 spacing, R_1–R_2 spacing, structure of antenna and transmitted signal frequency on the tool response were discussed, and the electromagnetic response of resistivity LWD tool in tilted anisotropic formation was also calculated.

Theory and mathematical modeling

Figure 1 shows the basic structure model of a resistivity LWD tool. In Fig. 1, T is the transmitter coil, R_1 and R_2 denote two receiver coils, L_1 (T–R_1 spacing) is the distance from T to R_1, L_2 (R_1–R_2 spacing) is the distance from R_1 to R_2, r is the radius of the transmitter coil and n_1 denotes the number of transmitter coil turns, $r_{\mathrm{R\ is}}$ the radius of the receiver coil and n_2 is the number of receiver coil turns, $\boldsymbol{I}_{\mathrm{T}}$ is excitation current intensity in the transmitter coil and $\boldsymbol{I}_{\mathrm{T}} = \boldsymbol{I}e^{i\omega t}$.

For resistivity LWD tool, the transmitter coil can be considered as an excitation source, and the alternating current in the transmitter coil may produce a high-frequency electromagnetic field around the wellbore. The electric field and magnetic field may reciprocally transform each other in space. Assuming that the resistivity LWD tool operates at a high-frequency condition, because the induced electromotive force of the receiving coils is generated by the alternating current, the solving electromagnetic field is a time-harmonic field. As the alternating current exists in the interior of the transmitter coil, a time-varying magnetic field must exist in the formation around the wellbore; thus, the induced magnetic field near the receiver coils should be a time-harmonic electromagnetic field. Based on the Maxwell equation, the wave equation of electric field $\boldsymbol{E}$ in anisotropic formation can be obtained and shown in Eq. (1):

$$\Delta \times \left(\frac{1}{\mu_{\mathrm{r}}}\Delta \times \boldsymbol{E}\right) - k_0^2 \varepsilon_r \boldsymbol{E} = -j\omega\mu_0 \boldsymbol{J}, \tag{1}$$

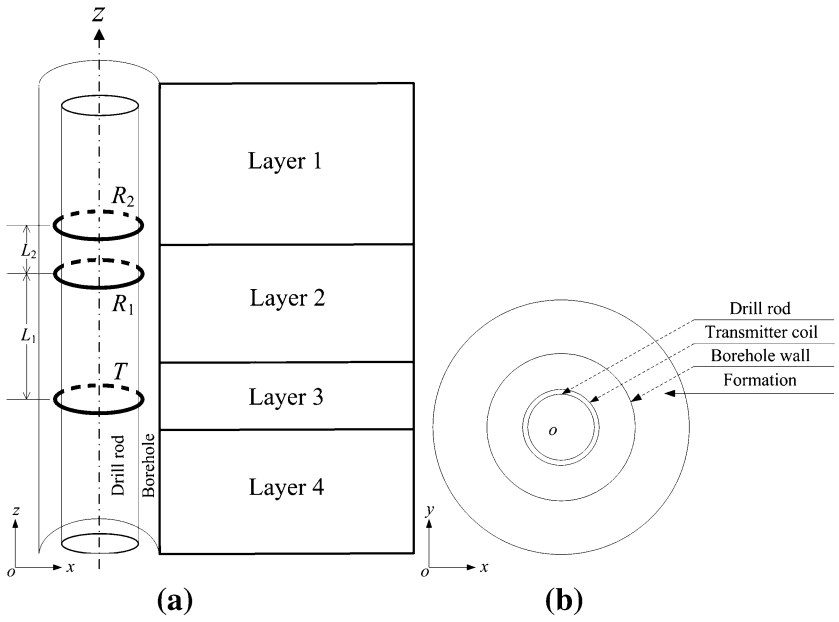

Fig. 1 Model of the resistivity LWD tool. **a** The basic structure of the resistivity LWD tool (*Oxz* axis). **b** The electromagnetic field analysis model with drill rod, transmitter coil, borehole wall and formations (*Oxy* axis)

where $\boldsymbol{E}$ denotes the electric field, ε_r denotes the composite dielectric constant, μ_r and μ_0 denote the relative magnetic permeability and permeability of free space, respectively, and k_0 denotes the wave number. Using Eq. (1), we can obtain the functional expression,

$$F(\boldsymbol{E}) = \frac{1}{2}\iiint_V \left[\frac{1}{\mu_r}(\Delta \times \boldsymbol{E}) \cdot (\Delta \times \boldsymbol{E}) - k_0^2 \boldsymbol{E} \cdot \varepsilon \cdot \boldsymbol{E}\right] \mathrm{d}V + j\omega\mu_0 \iiint_V \boldsymbol{E} \cdot \boldsymbol{J} \mathrm{d}V, \tag{2}$$

where V denotes the solution domain of the finite element.

According to Eq. (2), we can get

$$F(\boldsymbol{E}) = \sum_{e=1}^{M} F_e(\boldsymbol{E}) = \frac{1}{2}\sum_{e=1}^{M} \iiint_V \left[\frac{1}{\mu_r}(\Delta \times \boldsymbol{E}) \cdot (\Delta \times \boldsymbol{E}) - k_0^2 \boldsymbol{E} \cdot \varepsilon_r \cdot E\right] dV - j\omega\mu_0 \sum_{e=1}^{M} \iiint_V \boldsymbol{E} \cdot J \mathrm{d}V, \tag{3}$$

where e denotes the each split unit, M the total number of units, and J the Jacobian factor.

In each unit, the curl of scattered field can be expressed as

$$\Delta \times \boldsymbol{E} = \sum_{i=0}^{N_u-1}\sum_{j=0}^{N_v}\sum_{k=0}^{N_w} a_{uijk}\Delta \times \boldsymbol{f}_{uijk} + \sum_{i=0}^{N_u}\sum_{j=0}^{N_v-1}\sum_{k=0}^{N_w} a_{vijk}\Delta \times \boldsymbol{f}_{vijk} + \sum_{i=0}^{N_u}\sum_{j=0}^{N_v}\sum_{k=0}^{N_w-1} a_{wijk}\Delta \times \boldsymbol{f}_{wijk}, \tag{4}$$

where the curl of the basis function can be expressed as

$$\begin{cases} \Delta \times \boldsymbol{f}_{uijk} = \dfrac{1}{J}\left[u^i P_j(v)\dfrac{\mathrm{d}P_k(w)}{\mathrm{d}w}\cdot\dfrac{\mathrm{d}\boldsymbol{r}}{\mathrm{d}v} - u^i\dfrac{\mathrm{d}P_j(v)}{\mathrm{d}v}P_k(w)\cdot\dfrac{\mathrm{d}\boldsymbol{r}}{\mathrm{d}w}\right] \\ \Delta \times \boldsymbol{f}_{vijk} = \dfrac{1}{J}\left[v^j P_k(w)\dfrac{\mathrm{d}P_i(u)}{\mathrm{d}u}\cdot\dfrac{\mathrm{d}\boldsymbol{r}}{\mathrm{d}w} - v^j\dfrac{\mathrm{d}P_k(w)}{\mathrm{d}w}P_i(u)\cdot\dfrac{\mathrm{d}\boldsymbol{r}}{\mathrm{d}u}\right] \\ \Delta \times \boldsymbol{f}_{wijk} = \dfrac{1}{J}\left[w^k P_i(u)\dfrac{\mathrm{d}P_j(v)}{\mathrm{d}v}\cdot\dfrac{\mathrm{d}\boldsymbol{r}}{\mathrm{d}u} - w^k\dfrac{\mathrm{d}P_i(u)}{\mathrm{d}u}P_j(v)\cdot\dfrac{\mathrm{d}\boldsymbol{r}}{\mathrm{d}v}\right] \end{cases} \tag{5}$$

Substitution of Eqs. (5) and (4) into Eq. (3) gives

$$F(\boldsymbol{E}) = \frac{1}{2}\sum_{e=1}^{M} (a^e)^{\mathrm{T}} K^e a^e - \sum_{e=1}^{M} (a^e)^{\mathrm{T}} b^e, \tag{6}$$

where K^e denotes the unit matrix and b^e the vector.

$$K^e = \iiint_{V^e} \left[\frac{1}{\mu_{\mathrm{r}}^e}(\Delta \times \boldsymbol{f}^e) \cdot (\Delta \times \boldsymbol{f}^e)^{\mathrm{T}} - k_0^2 \boldsymbol{f}^e \cdot \varepsilon_r^e \cdot (\boldsymbol{f}^e)^{\mathrm{T}}\right] \mathrm{d}V, \tag{7}$$

$$b^e = -j\omega\mu_0 \iiint_{V^e} [\boldsymbol{f}^e \cdot J] \mathrm{d}V. \tag{8}$$

According to Eq. (6), we can get the linear equations

$$Ax = B, \tag{9}$$

where $A = \sum_{e=1}^{M} K^e$, $x = \sum_{e=1}^{M} a^e$ and $b = \sum_{e=1}^{M} b^e$. Solving Eq. (9), the electric field $\boldsymbol{E}$ at each measurement point can be obtained.

Instrument parameter calibration

When an electromagnetic wave propagates in the porous media near the wellbore formation, the signal amplitude attenuation is different because there are different resistivities among different propagation media. Based on that, by detecting the amplitude ratio and phase difference of induction electromotive force received by two receiver coils mounted on the resistivity LWD tool, the resistivities of different media can be obtained according to the measurement model of the tool. The antenna system is the most important part in the resistivity LWD tool, which includes an electromagnetic wave transmitter and receiver sensors. The detection depth and resolution are influenced by the coil spacing of the antenna system. The basic structures of the resistivity LWD tool and the formation model are shown in Fig. 1. The drill collar is highly conductive, and the transmitter and receiver coils are equipped with a magnetic buffer at 10^{-4} S/m. The relative permeability is 10^4, the conductivity of the drill collar is 10^6 S/m, the conductivity of mud in the borehole is 10 S/m, the vertical depth of the formation model z is equal to 9.0 m, and the relative dielectric constant of formation ε_r is equal to 1. The conductivity of each layer is shown in Table 1.

T–R_1 spacing of the antenna system

The initial T–R_1 spacing is L_1, which is equal to 0.4 m, and the initial R_1–R_2 spacing is L_2, which is equal to 0.2 m. The transmitting frequency f is equal to 2 MHz, and the excitation current intensity $\boldsymbol{I}_{\mathrm{T}}$ is equal to 1.0 A. By using

Table 1 Parameters of the formation model

Layer number	Horizontal conductivity σ_{h}/(S/m)	Vertical conductivity σ_{v}/(S/m)	Interface z (m)
1	0.001	0.0067	3.0
2	0.01	0.05	5.0
3	0.001	0.005	6.0
4	0.01	0.0167	9.0

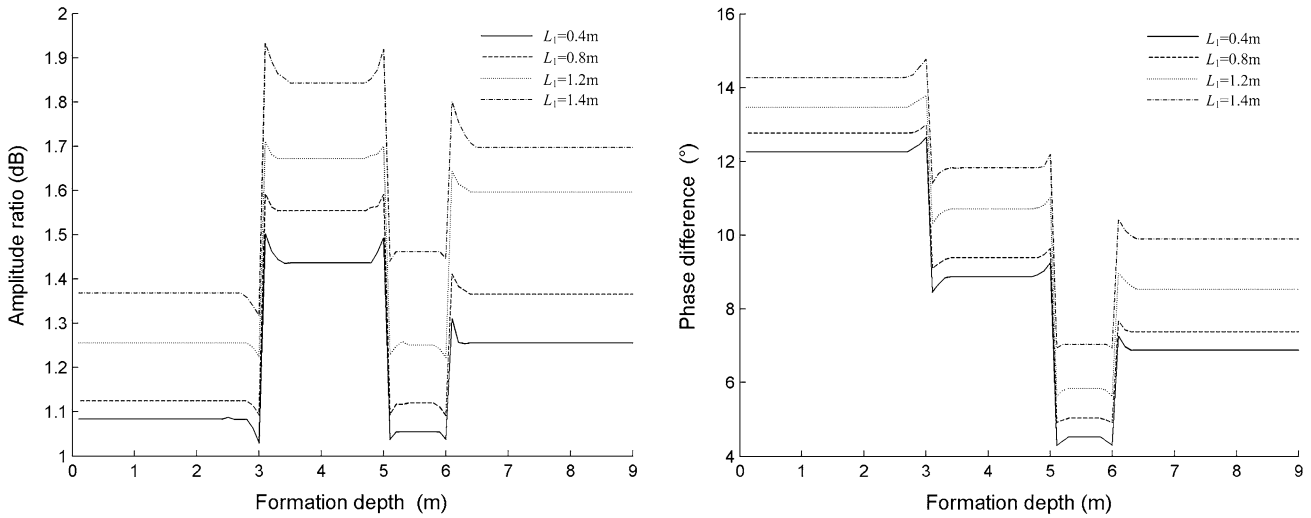

(a) amplitude ratios **(b)** phase differences

Fig. 2 Amplitude ratios and phase differences by changing the T–R_1 spacing

higher-order vector FEM to build the numerical model, we fix the distance of two receiver coils, change the T–R_1 spacing L_1, and then investigate the measurement results of the resistivity LWD tool. When L_1 is equal to 0.4, 0.8, 1.2 and 1.4 m, respectively, the corresponding amplitude ratios and phase differences of the electromagnetic wave signal received by two receiver coils are shown in Fig. 2.

In Fig. 2, the amplitude ratios and phase differences of electromagnetic wave signals received by two receiver coils are increased when the T–R_1 spacing of antenna system is increased, but the phase differences are not influenced by T–R_1 spacing strongly. When the T–R_1 spacing increases between 0.4 and 1.4 m, the polarization angles emerge in the formation interface of the amplitude ratios and phase difference curves noticeably. When T–R_1 spacing is larger than 1.2 m, in the high-resistivity thin layer, the polarization angles are not clear enough in amplitude ratios and the phase difference curves because of the influence of the skin effect on receiving signals.

R_1–R_2 spacing of the antenna system

The initial R_1–R_2 spacing is L_2, which is equal to 0.2 m; the transmitting frequency f is equal to 2 MHz, and the excitation current intensity $\boldsymbol{I}_T$ is equal to 1.0 A. We fix the T–R_1 spacing, which is equal to 0.8 m, change the R_1–R_2 spacing L_2, and then investigate the measurement results of the resistivity LWD tool. When L_2 is equal to 0.2, 0.6, 1.0 and 1.2 m, respectively, the corresponding amplitude ratios and phase differences of the electromagnetic wave signal received by two receiver coils are shown in Fig. 3.

In Fig. 3, in the high-resistivity layer, the amplitude ratios of electromagnetic wave signals received by two receiver coils increased when the R_1–R_2 spacing of the antenna system is increased. But in the low-resistivity layer, the amplitude ratios decreased when the R_1–R_2 spacing of the antenna system increased. The phase differences of the electromagnetic wave signals received by two receiver coils increased when the R_1–R_2 spacing of the antenna system increased. When the R_1–R_2 spacing increased between 0.2 and 1.2 m, the polarization angles which emerged in the formation interface of the amplitude ratios and phase difference curves were not clear enough. That is to say, by using amplitude ratios and phase differences curve, we cannot indicate the formation interface accurately and timely. With the increase of R_1–R_2 spacing, the resolution of the resistivity LWD tool is decreased, especially to the high-resistivity thin layer. That is to say, such a situation is unfavorable to perform geosteering drilling and thin-layer resolution. It can be seen from Figs. 2 and 3 that the change in the T–R_1 spacing of the antenna system has obvious influence on the investigation depth and formation resolving power of the resistivity LWD tool. The change in the R_1–R_2 spacing can influence the resolution and geosteering capabilities of the resistivity LWD tool. Therefore, the detection accuracy and detection depth of the resistivity LWD tool would be strongly affected by the antenna system. Based on numerical experiments, we obtain that the optimum T–R_1 spacing is equal to 0.8 m, and the optimum R_1–R_2 spacing is equal to 0.2 m.

Transmitting frequency of the antenna system

According to the measurement results of "T–R_1 spacing of antenna system" and "R_1–R_2 spacing of antenna system",

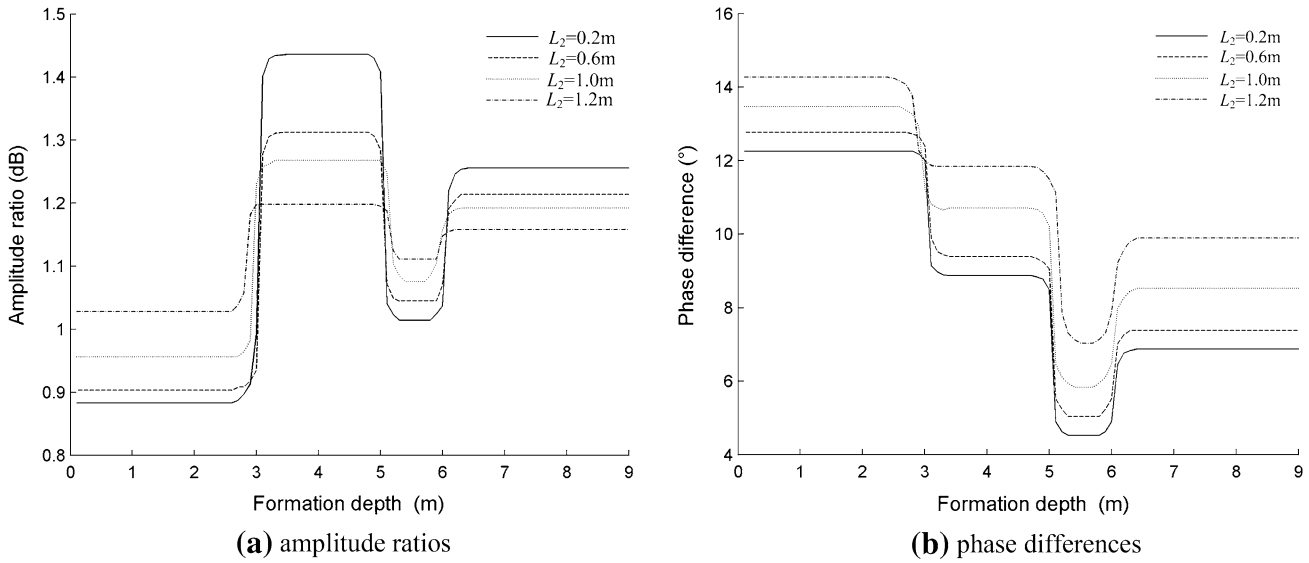

Fig. 3 Amplitude ratios and phase differences by changing the R_1–R_2 spacing

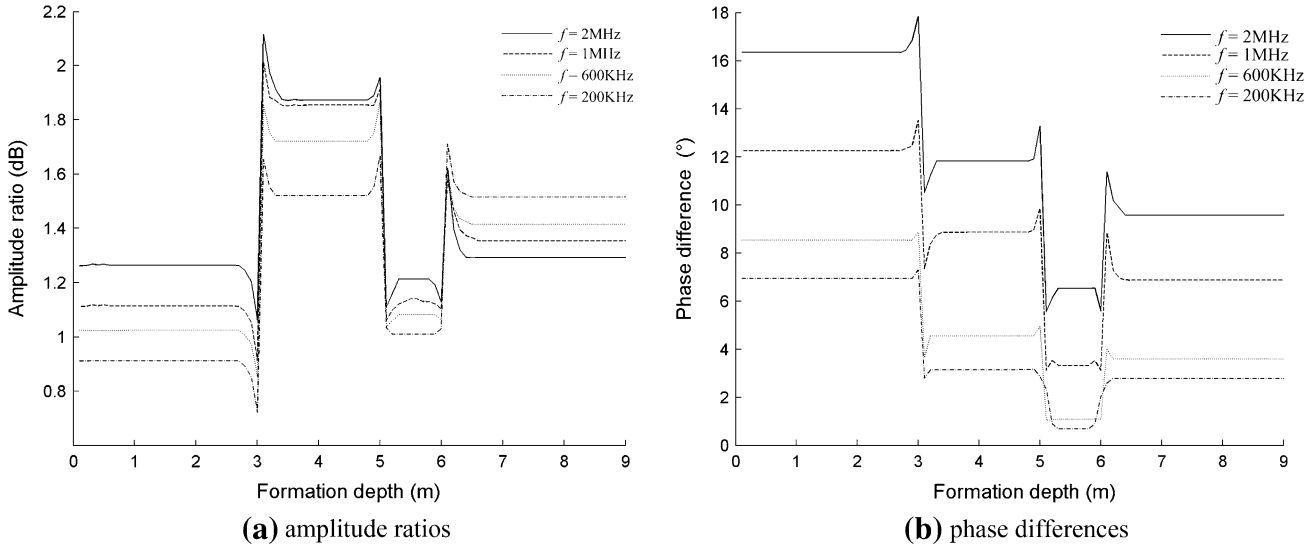

Fig. 4 Amplitude ratios and phase differences by changing the transmitting frequency

we obtain that the optimum T–R_1 spacing is equal to 0.8 m and the optimum R_1–R_2 spacing is equal to 0.2 m. So, we fix the T–R_1 spacing and R_1–R_2 spacing. When L_1 is equal to 0.8 m and L_2 is equal to 0.2 m, we change the transmitting frequency to investigate the response of the resistivity LWD tool. When the transmitting frequency f is equal to 200, 600 kHz, 1 and 2 MHz, respectively, the measurement results of the amplitude ratios and the phase differences of electromagnetic wave signal received by two receiver coils are shown in Fig. 4.

Figure 4 shows that the amplitude ratios and phase differences of the signals in two receiver coils increase gradually as the transmitting frequency increases from 200 kHz to 2 MHz, and the variations are more obvious in the case of low-resistivity formation. When the transmitting frequency is larger than 600 kHz, the polarization angle emerge in amplitude ratios and phase difference curves noticeably. According to Fig. 4, we find that the optimum transmitting frequency is equal to 2 MHz, because when f is equal to 2 MHz the amplitude ratios and phase difference curves have the best resolution. When the transmitting frequency is fixed at 2 MHz and the dielectric constant of an earth formation is changed during the procedure of numerical simulation, there are also changes in the amplitude ratios and phase differences of the receiving signal and these variations in the high-resistivity formation

are more sensitive than in low-resistivity formation. However, increase the transmitting frequency can enhance the detection resolution of low-resistivity formation, but the transmitting frequency is not the larger the better. Because with the the increase of the transmitting frequency, the calculated amount of higher-order vector FEM must increase, the computation errors may also increase. In practice, improvement in the transmitting frequency may lead to skin effect influence on the transmitter coil and receiving signals; therefore, the precision of the measurement results will be impacted.

Skin effect of the antenna system

In practice, the high-resistivity layer is generally the oil layer, so we can use the resistivity LWD tool to find the high-resistivity layer. But the resolution and accuracy of the resistivity LWD tool decide the accuracy of the measurement results, especially the high-resistivity thin layer. Therefore, the high precision resistivity LWD tool should be designed, and the antenna system is a key part in the design of the tool. Because the actual instrument structure is fixed and it is hard to be changed, such as T–R_1 spacing and R_1–R_2 spacing, the transmitting frequency can be easily adjusted. Based on "Transmitting frequency of antenna system", we obtain that if the transmitting frequency is low, the current is uniformly distributed in the internal parts of the transmitter coil, and the transmitter coil is not strongly affected by the skin effect. In conditions of high frequency, the current gradually concentrates on the surface of the transmitter coil and the internal current of the transmitter coil is obviously decreased. That is to say, the maximum current density is distributed at the surface of the transmitter coil. Therefore, in the condition of high frequency, the transmitter coil is strongly affected by the skin effect. So, in the high-frequency condition, the influence of the skin effect should be considered.

In "T–R_1 spacing of antenna system", "R_1–R_2 spacing of antenna system and "Transmitting frequency of antenna system", we obtain that in the antenna system the optimum T–R_1 spacing is equal to 0.8 m, the optimum R_1–R_2 spacing is equal to 0.2 m, and the optimum transmitting frequency is equal to 2 MHz. Therefore in this section, we use these optimum parameters to build up the numerical model. As the resistivity LWD tool moves along the vertical direction (z-axis) in a borehole, when $z = 5.5$ m (high-resistivity thin layer) and the transmitting frequency f is equal to 200, 600 kHz, 1 and 2 MHz, respectively, the distribution of the electric field to each transmitting frequency is shown in Fig. 5.

It is shown in Fig. 5 that as the transmitting frequency increases, the detection depth of the instrument also increases. As the transmitting frequency increases from 200 kHz to 2 MHz, the induced electric field around the

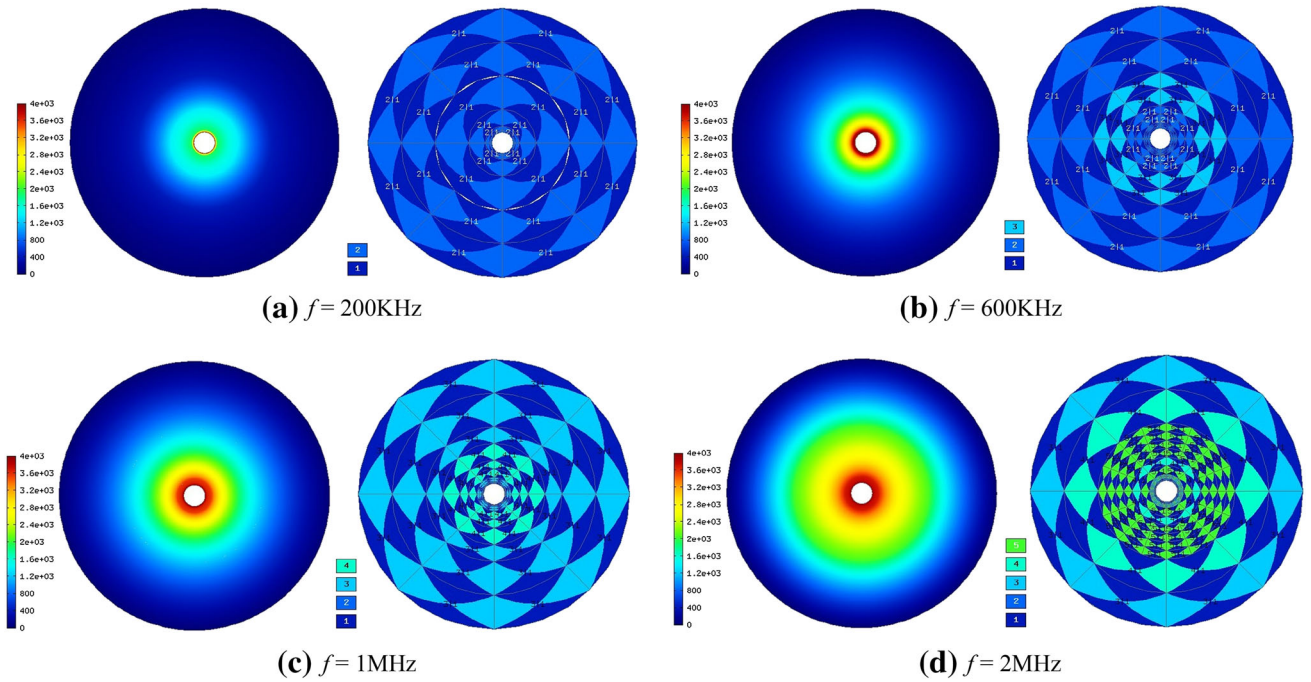

Fig. 5 Potential distribution and mesh subdivision. **a–d** The *left plot* represents the distribution of the electric field (unit: V/m) around the transmitting coil in the high-resistivity thin layer; the *right plot* represents the final mesh by using the higher-order vector finite element method (*Oxy* axis and $z = 5.5$ m). *Different colors* indicate different polynomial orders of approximation, ranging from 1 to 5; the transmitting frequency f is equal to 200, 600 kHz, 1 and 2 MHz, respectively

transmitter coil is significantly enhanced. When the transmitting frequency is low, such as 200 kHz, the transmitting current is evenly distributed within the transmitting coils, and the higher-order vector FEM needs less degree of freedoms, calculation time and iterative numbers to compute the electric field strength in the computational domain. When the transmitting frequency is high, such as 2 MHz, and the transmitting current is gradually concentrated on the transmitter coil surface, then the transmitter coils may be influenced by the skin effect noticeably. The higher-order vector FEM needs more degrees of freedom, calculation time and iterative numbers to compute the electric field strength in the computational domain. However, in the high-frequency condition, the higher-order vector FEM needs more degrees of freedom, calculation time and so on. That is to say, this may increase the calculation error. In practice, the detection depth of the resistivity LWD tool is an important performance indicator, and the mud filtrate in the borehole has a certain degree of absorption of electromagnetic signal, which may reduce the induced electric field strength around the transmitter coil and reduce the detection accuracy and detection depth of the tool. Therefore, the transmitting frequency should be increased. But when the transmitting frequency is too high, a part of the current will be dissipated in the form of heat in the transmitter coil, which may lead to significantly reduced electromagnetic signal intensity, thus the detection accuracy and detection depth of the instrument may be strongly affected. When the transmitting frequency f is equal to 400, 800 kHz, 1, 2 and 5 MHz, respectively, the measurement results of the real part and imaginary part of the electromagnetic wave signals received by one receiver coil are shown in Fig. 6.

It is shown in Fig. 6 that with the increases of transmitting frequency, the real part of the electromagnetic wave signals received by the receiver coil R_1 increases, but the imaginary part of the electromagnetic wave signals received by the receiver coil R_1 decreases. That is to say, with the increases of transmitting frequency, the resolution of instrument to the high-resistivity thin layer will gradually increase. When the transmitting frequency f is equal to 5 MHz, the imaginary part of electromagnetic wave signals is not approximately a straight line, that is to say, the transmitter coil is strongly affected by the skin effect. As the transmitting frequency increases, the potential differences received by two receiver coils gradually increase, and then at the interface of formations the distribution of electric field is uneven. Therefore, the polarization angle emerging in amplitude ratios and phase differences are easily influenced by different transmitting frequencies. If the transmitting frequency is very large, the transmitter coil may be noticeably affected by the skin effect; so it may lead to the distortion caused by the polarization angle, which may affect the accuracy of the measurement results.

Geosteering capabilities of the resistivity LWD tool

When an electromagnetic wave propagates in the porous media near the borehole formation, the signal amplitude attenuation is different because there are different resistivities among different propagation mediums. Based on

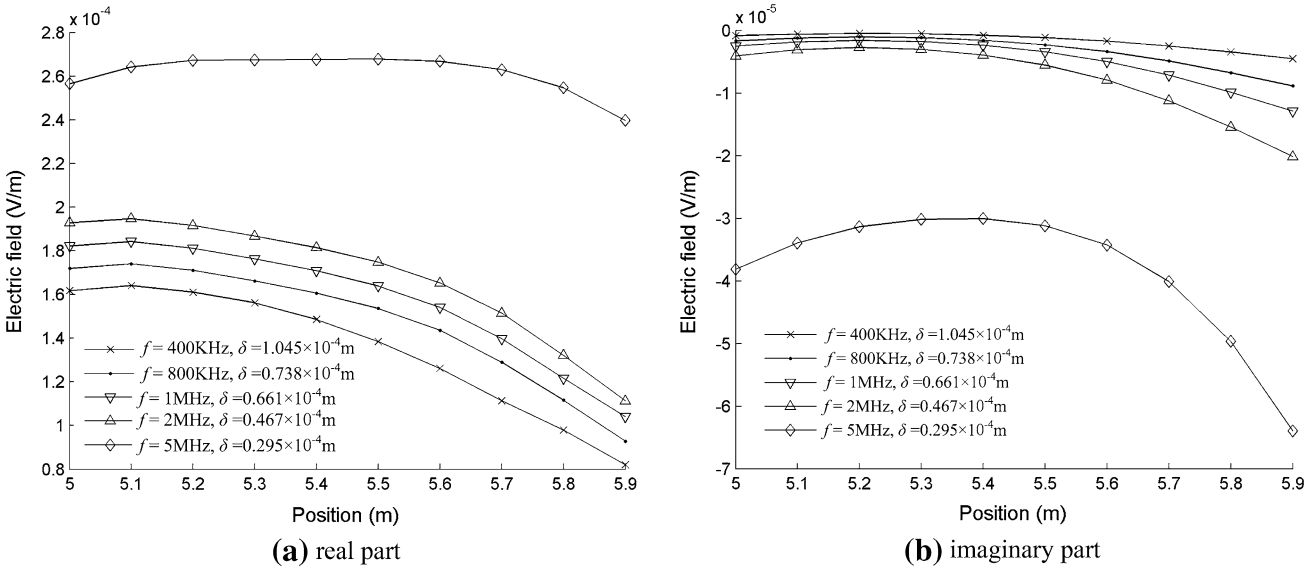

(a) real part **(b)** imaginary part

Fig. 6 Real part and imaginary part curves of the receiver coil R_1 at $f = 400$ kHz, $\delta = 1.045 \times 10^{-4}$ m; $f = 800$ kHz, $\delta = 0.738 \times 10^{-4}$ m; $f = 1$ MHz, $\delta = 0.661 \times 10^{-4}$ m; $f = 2$ MHz, $\delta = 0.467 \times 10^{-4}$ m; $f = 5$ MHz, $\delta = 0.295 \times 10^{-4}$ m. Here, f denotes the transmitting frequency and δ the skin depth

that, by detecting the amplitude ratios and phase differences of induction electromotive force received by two receiver coils mounted on the resistivity LWD tool, the resistivities of different media can be reflected according to the measurement model of the tool.

Influence of tilted formation

The structure of the resistivity LWD tool is shown in Fig. 7. In Fig. 7, the drill collar is highly conductive, and the transmitter and receiver coils are equipped with a magnetic buffer at 10^{-4} S/m. The relative permeability is 10^4, the conductivity of the drill collar is 10^6 S/m and the conductivity of the mud in the borehole is 10 S/m. According to "T–R_1 spacing of antenna system", "R_1–R_2 spacing of antenna system", "Transmitting frequency of antenna system" and "Skin effect of antenna system", we obtain that in the antenna system the optimum T–R_1 spacing is equal to 0.8 m, the optimum R_1–R_2 spacing is equal to 0.2 m, the optimum transmitting frequency is equal to 2 MHz and the optimum excitation current intensity $\boldsymbol{I}_T$ is equal to 1.0 A. Therefore, in this section we use these optimum parameters to build up the numerical model. The conductivity of each formation is shown in Table 1.

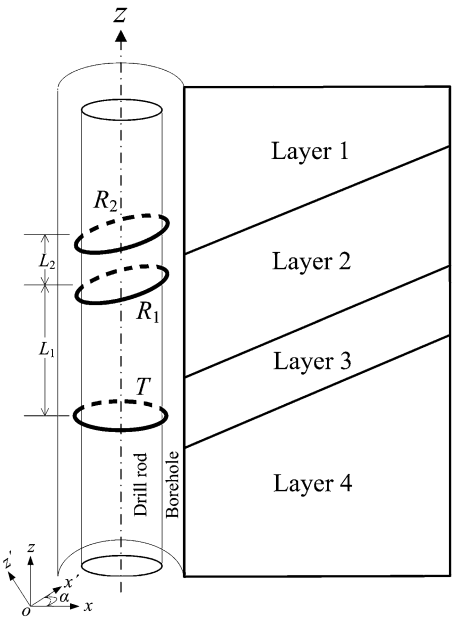

Fig. 7 Structure of the resistivity LWD tool in tilted formation (*Oxz* axis)

Assume that the resistivity LWD tool moves upward along a vertical direction (z-axis) in a borehole. As receiver coils are placed without any tilt around a cylindrical steel mandrel, the dip angle α of the formation is equal to 15°, 30°, 45° and 60°, respectively. The amplitude ratios and the phase differences of the electromagnetic wave signal received by two receiver coils are shown in Fig. 8.

Generally, we can provide timely geosteering drilling information according to the polarization angles whether appearing on the amplitude ratio curves or the phase difference curves corresponding to the interface between two formations. It can be seen from Fig. 8 that although there are narrow polarization angles occurring in the amplitude ratio and the phase difference curves, respectively, because the polarization angles appear on the curves corresponding to both the interface from low-resistivity formation to high-resistivity formation and the interface from high-resistivity formation to low-resistivity formation, it is very difficult to

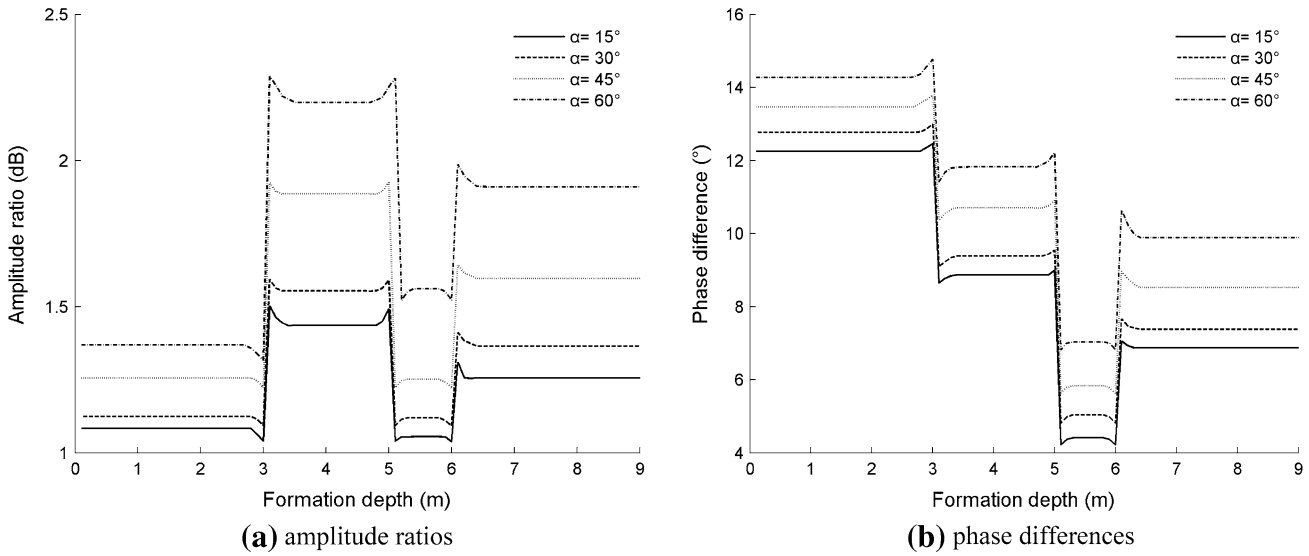

Fig. 8 Amplitude ratios and phase differences in tilted formation

determine the drilling direction in time. Therefore, as the receiver coils are placed without any tilt around a cylindrical steel mandrel, the geosteering drilling information cannot be provided accurately.

Directional resistivity LWD in the tilted formation

Assume that the transmitter coil is placed without any tilt around a cylindrical steel mandrel and the two receiver coils are tilted by about 45° with respect to the cross section of the cylindrical steel mandrel. In that case, considering that the dip angle α of the tilted formation is equal to 15°, 30°, 45° and 60°, respectively, the amplitude ratios and the phase differences of the electromagnetic wave signal received by two receiver coils are shown in Fig. 9.

It is shown in Fig. 9 that tilts of the two receiver coils can affect the judgment of low-resistivity formation and high-resistivity formation. In the condition of tilted receiver coils, when the dip angle of the formation increases, the resolution of instrument measurement results in the low-resistivity formation and high-resistivity formation gradually increasing. According to the polarization angles in amplitude ratios and phase difference curves, we can indicate the interface between the two formations clearly. However, as shown in Fig. 9, with the increase of dip angle of the formation, the variations of amplitude ratios and phase differences received by two receiver coils all present an upward trend. But in amplitude ratios and phase difference curves, we can find that with the increase of dip angle of the formation, the polarization angles corresponding to the interface from low-resistivity formation to high-resistivity formation gradually disappear. Conversely, the polarization angles corresponding to the interface from high-resistivity formation to low-resistivity formation become more and more obvious. Based on that, the drilling direction can be determined in time according to the polarization angles whether appear on the amplitude ratios and the phase difference curves corresponding to the interface between two formations, then the geosteering drilling information can be accurately provided by resistivity LWD tool.

Table 2 Instrument response of the resistivity LWD tool

α (°)	Average value of measurement results			
	D	*T* (s)	*N* (time)	*P* (%)
15	27,138	9.59	10	0.65
30	33,167	11.73	13	0.77
45	49,272	25.66	17	0.82
60	57,163	30.15	22	0.93

Based on the higher-order vector FEM, the numerical simulation model of the resistivity LWD tool can be built, and when the dip angle α of the tilted formation is equal to 15°, 30°, 45° and 60°, respectively, the average value of measurement results of the resistivity LWD tool are shown in Table 2, where *D* denotes the degrees of freedom, *T* the calculation time, *N* the iterative numbers and *P* the global errors.

It can be seen from Table 2, by using higher-order vector FEM to build the simulation model of resistivity LWD tool and calculate the electric field strength around the receiver coils, when the dip angle of formation $\alpha = 15°$, the model needs an average number of DOFs used in calculation of 27,138; the average calculation time is 9.59 s; the average number of iterations is 10, and the

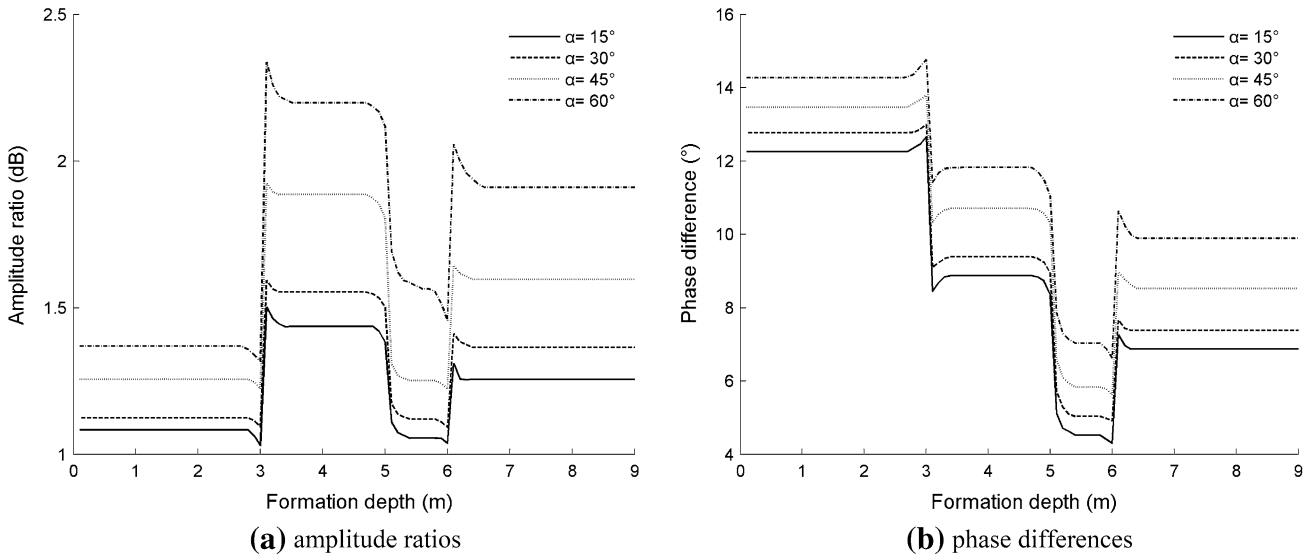

(a) amplitude ratios **(b)** phase differences

Fig. 9 Amplitude ratios and phase differences in tilted formation with tilted receiver coils

average global error is 0.65 %. When the dip angle of formation $\alpha = 30°$, the model needs an average number of DOFs used in the calculation of 33,167; the average calculation time is 11.73 s; the average number of iterations is 13, and the average global error is 0.77 %. When the dip angle of formation $\alpha = 45°$, the model needs an average number of DOFs used in calculation of 49,272; the average calculation time is 25.66 s; the average number of iterations is 17, and the average global error is 0.82 %. When the dip angle of formation $\alpha = 60°$, the model needs an average number of DOFs used in the calculation of 57,163; the average calculation time is 30.15 s; the average number of iterations is 22, and the average global error is 0.93 %. In Table 2, when the dip angle of formation $\alpha = 60°$, the model needs more DOF, calculation time, iterations and global errors. Because in order to ensure a higher solution accuracy, the grids refinement at the regions with a strong electric field changes and at the interface of formations would be strengthen, therefore a large amount of DOFs and calculation time would be used.

Conclusions

In this paper, by using higher-order vector FEM, we have successfully investigated the impact of the measurement results by changing the T–R_1 spacing, R_1–R_2 spacing, transmitting frequency and the structure of resistivity LWD tool. The antenna system is the important part of the resistivity LWD tool, and the measurement results of the instrument would be strongly affected by different T–R_1 spacing, R_1–R_2 spacing and transmitting frequency. Numerical simulation results show that the change of T–R_1 spacing has obvious influence on the investigation depth and detecting precision of the resistivity LWD tool, and the change of R_1–R_2 spacing may affect the resolution of the thin-layer distinguish. The change of signal source transmitting frequency can influence the judgment of the formation interface, and high transmitting frequency can improve the instrument resolution of high-resistivity thin layer. The structure of the antenna system can also affect the measurement results of the resistivity LWD tool, and we can use the asymmetry of polarization angles that appear on the amplitude ratios and the phase difference curves to provide accurate geosteering drilling information.

In practice, because the geological condition around the wellbore is complex, it may affect the electromagnetic response of the resistivity LWD tool, so that the instrument parameters need to be adjusted. Thus, it can be seen that the study of the numerical simulation for resistivity LWD tool response has important significance to guide the development of high-precision resistivity LWD tool and build accurate resistivity LWD measurement data interpretation method. But by using conventional resistivity LWD tool logging curve, field engineers are hard to judge the bit position, also the reservoir drilling rate must be declined. But directional resistivity LWD tool logging curve can provide the bit position information, well deviation information, azimuth information and tool surface information; thus the directional resistivity LWD tool is important for the directional drilling construction operation, and the next research focusing on the resistivity LWD tool will optimize the structure of the tool, reducing the length of the instrument and improving the performance index of the tool.

Acknowledgments This project was supported by the National Natural Science Foundation of China (No. 61475027), Natural Science Foundation of Chang zhou Institude of Technology (No.YN1208).

References

Babuška I, Suri M (1987) The hp-version of the finite element method with quasiuniform meshes. Math Model Numer Anal 21:199–238

Chen X, Liu D, Ma Z (2011) Numerical simulation of electric field in resistivity LWD using high accuracy self-Adaptive hp-FEM. Chin J Comput Phys 28:50–56

Demkowicz L, Vardapetyan L (1998) Modeling of electro-magnetic absoption scattering problems using hp-adaptive finite elements. Comput Methods Appl Mech Eng 152:103–124

Demkowicz L, Rachowicz W, Devloo P (2002) A fully automatic hp-adaptivity. J Sci Comput 17:117–142

Gao J, Ke S, Wei B (2010) Introduction to numerical simulation of electrical logging and its development trend. Well Logging Technol 34:2–4

Hue YK, Teixeira FL, Martin LS et al (2005) Three-dimensional simulation of eccentric LWD tool response in boreholes through dipping formations. IEEE Trans Geosci Remote Sens 43:257–268

Li J, Liu C (2005) Three-dimensional transmission line matrix method (TLM) for simulation of logging tools. IEEE Trans Geosci Remote Sens 38:1522–1529

Li H, Liu D, Liu Y et al (2012) Application of self-adaptive hp-FEM in numerical simulation of resistivity logging-while-drilling. Chin J Geophys 55:2787–2797

Ma Z, Liu D, Li H et al (2012) Numerical simulation of a multi-frequency resistivity logging-while-drilling tool using a highly accurate and adaptive higher-order finite element method. Adv Appl Math Mech 4:439–453

Pardo D, Demkowicz L, Torres-Verdín C (2007) A self-adaptive goal-oriented hp finite element method with electromagnetic applications. Part II: electrodynamics. Comput Methods Appl Mech Eng 196:3585–3597

Shi P (2002) LWD technology plays an important role in China oilfield development. Well Logging Technol 26:441–445

Šolín P, Červený J, Doležel I (2008) Arbitrary-level hanging nodes and automatic adaptivity in the hp-FEM. Math Comput Simul 77:117–132

Sun X, Nie Z, Zhao Y (2008) The electromagnetic modeling of logging-while-drilling tool in tilted anisotropic formations using vector finite element method. Chin J Geophys 51:1600–1606

Tan M, Zhang G, Lian H et al (2007) 3-D numerical mode-matching (NMM) method for resistivity logging responses in nonsymmetric conditions. Chin J Geophys 50:945–949

Teixeiraa FL, Chew WC (2004) Finite difference modeling of electromagnetic tool response for logging while drilling. Geophysics 69:152–160

Tomáš V, Pavel S, Martin Z et al (2007) Modular hp-FEM system HERMES and its application to Maxwell's equations. Math Comput Simul 76:223–228

Wang R, Wang M, Di Q (2006) Electromagnetic modeling due to line source in frequency domain using finite element method. Chin J Geophys 49:1858–1866

Wei B, Tian K, Zhang X et al (2010) Evaluating influence of eccentricity on response of electromagnetic wave resistivity logging-while-drilling by vector eigenfunction expansion formulae for dyadic Green's functions. J China Univ Pet 34:57–62

Zhang Z, Liu Q (2003) Applications of the BCGS-FFT method to 3-D induction well-logging problems. IEEE Trans Geosci Remote Sens 41:998–1004